periodica polytechnica

Electrical Engineering and Computer Science
56/3 (2012) 83–94
doi: 10.3311/PPee.7079
http://periodicapolytechnica.org/ee
Creative Commons Attribution

RESEARCH ARTICLE

Data fusion and primary image processing for aircraft identification

Loránd Lukács / *Béla* Lantos

Received 2012-06-25, revised 2012-10-11, accepted 2012-10-12

Abstract

The primary scope of this study lays on system technique solutions of collecting data required for the identification of an aircraft's nonlinear dynamic model.

It is assumed that the aircraft has no inbuilt navigational system, nor any sensors mounted on its control surfaces. The control column and pedals manipulated by the pilot can only visually be observed. For the time of data logging, an external sensory system (GPS, IMU) and a camera system were deployed on the airplane supporting the collection of flight data.

The paper presents the data acquisition solutions required for aircraft's nonlinear model identification, with an emphasis on the determination of the control surface positions as the system's input signals using image processing. During flight, the control column and pedal positions manipulated by the pilot are recorded using a video camera and with post processing, data is converted to control surface (rudder, elevator, aileron) positions. The 3D positions of the pilot's control column are determined from 2D pixel values. The input signals are then calculated using this information and the control surface characteristics. The input signals and state variables determined with a state estimator are regarded as input signals for the identification of an aircraft's nonlinear model.

Keywords

data fusion · camera calibration · image processing · state estimation · aircraft identification

Acknowledgement

This research was supported by the Hungarian National Research Program under grant No. OTKA K71762 project.

Our special thanks are due to Dr. Zoltán Prohászka and PhD candidate László Kis for their technical advices.

Loránd Lukács

Department of Control Engineering and Information Technology, BME, H-1117 Budapest, Magyar Tudósok krt. 2., Hungary

Béla Lantos

Department of Control Engineering and Information Technology, BME, H-1117 Budapest, Magyar Tudósok krt. 2., Hungary
e-mail: lantos@iit.bme.hu

1 Introduction

Airplanes are complex nonlinear dynamic systems. The development of a control system (autopilot etc.) needs the knowledge of the dynamic model and its parameters. The dynamic model can be determined using nonlinear identification methods based on the record of state variables and actuator signals belonging to real flight data:

$$\left\{\begin{array}{c}\text{state variables}\\ \text{actuator signals}\end{array}\right\} \xrightarrow{\text{identification}} \begin{array}{c}\text{dynamic}\\ \text{model}\end{array}$$

The state variables describe the position, velocity, orientation and angular velocity of the aircraft. The actuator signals consist of the positions of the control surfaces and the engine trust. The theory of identification of an aircraft's nonlinear dynamic model is discussed in detail in [1]. As can be seen, the system identification needs the state variables which can be determined based on the kinematic model and the fusion of GPS, IMU (Inertial Measurement Unit containing 3D accelerometer and 3D angular velocity sensors) and 3D magnetometer sensors by using stochastic state estimator or deterministic state observer methods:

$$\left\{\begin{array}{c}\text{sensor}\\ \text{signals}\end{array}\right\} \xrightarrow[\text{observer}]{\text{state estimator /}} \text{state variables}$$

Since the kinematic model is nonlinear hence the state estimator can use EKF (Extended Kalman Filter) with (possibly) external complementary filter loop [2]. Alternatively, deterministic nonlinear state observers can also be used based on Lyapunov stability theory [4] or transformation Lie-groups [5].

This study's primary focus is on system technique solutions of collecting data required for the identification of an aircraft's nonlinear dynamic model. It is assumed that the aircraft has no inbuilt navigational system, nor any sensors mounted on its control surfaces (rudder, elevator, aileron). The flight of the airplane is influenced by the control column and pedals manipulated by the pilot whose positions can visually be observed. This situation can often occur in the first phase of control system development of airplanes when no sensors are mounted on the control surfaces. On the other side, the design of the control system

needs the knowledge of the dynamic model, which can be identified from real flight data. Hence a sensory system (GPS, IMU, magnetometer) and a camera system have to be placed on the airplane supporting the collection of flight data for state estimation and model identification.

Special emphasis is on determining the system's input signals comprised of the aircraft's actuator positions with the aid of image processing:

$$\left\{ \begin{array}{c} \text{video} \\ \text{sequences} \end{array} \right\} \xrightarrow{\text{image processing}} \left\{ \begin{array}{c} \text{actuator} \\ \text{signals} \end{array} \right\}$$

where the video sequences contain the 2D pixel positions of the markers on the control column and pedals while the actuator signals have to contain the positions of the control surfaces (rudder, elevator, aileron).

Using a sailplane (glider) as an example, the study presents the data acquisition process required for state estimation and identification of an aircraft's nonlinear model, discussing in detail the determination of control surface positions using image processing. The theory and basics of image processing are discussed in [6].

The aircraft of choice was the R26-S Góbé, a two-seater sailplane (glider), taking into consideration that the lack of an engine considerably reduces the identification problem. Lacking an onboard navigation system and aircraft control position sensors means that the control surface positions have to be generated using image processing techniques. The results can be extended for use on engine-powered aircraft, laying the foundations of autopilot development in the future.

The aircraft's speed, position and orientation have been determined using a differential GPS module, accelerometer, angular velocity-meter and magnetometer, the fusion of which can lay the foundation of the estimation of the aircraft's states using extended Kalman filtering.

One of the differential GPS receivers was mounted on the nose of the aircraft, while the other one on the aircraft's body, close to its center of mass. For navigation purposes the usual ECI, ECEF, NED and ABC (Aircraft Body or shortly Body) coordinate systems (frames) are used, see Figure 1. We refer to the frames by the indexes i, e, n, b.

The signals belonging to the body frame are shown in Figure 2, where Φ, Θ, Ψ denote Euler (roll, pitch,yaw) angles, U, V, W are the velocity, P, Q, R the angular velocity, X, Y, Z the force and L, M, N the torque components, respectively, while v_T is the magnitude of the velocity, α is the angle of attack and β is the sideslip angle.

The control surfaces of a conventional airplane are shown in Figure 3.

Regarding the terminology of the paper, we speak about control column and pedal positions manipulated by the pilot and the positions of the control surfaces (elevator, aileron and rudder) as consequences of the pilot's manipulation. Between them

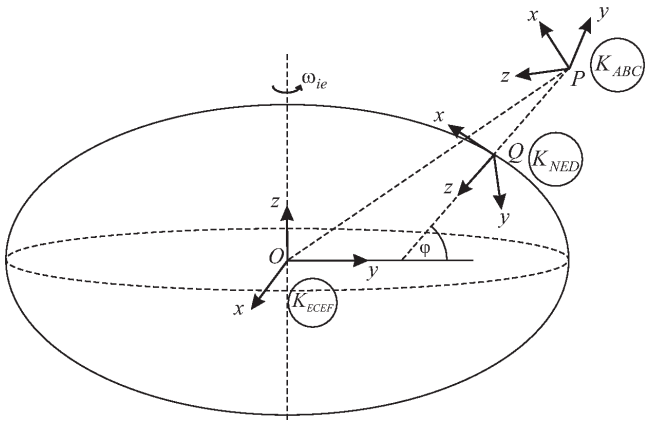

Fig. 1. Coordinate systems used in navigation

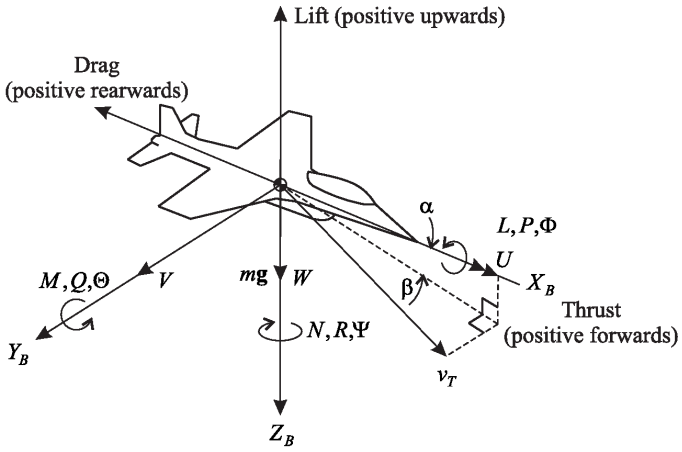

Fig. 2. The frame fixed to the airplane with the kinematic and force/torque variables

there is an unknown mechanical structure, however the (nonlinear) characteristics can be manually determined before flight. It is assumed that the control surfaces have no sensors.

On the other hand, the mechanical structure of the control column is assumed known and will be called the kinematic model of the control column. However, for the (joint) variables of this model no sensors are available. Hence, firstly the 3D positions of the control column have to be determined from their 2D coordinates on the image plane of a single camera. Then, using these 3D positions and the control surface characteristics, the positions of the elevator and aileron control surfaces can be computed. The procedure will be supported by a look-up table. The position of the control pedal can immediately be measured and converted to rudder position.

The structure of the paper is as follows. Section 2 describes the determination of the control surface characteristics. Section 3 presents the concept of data acquisition during flight. Section 4 describes the determination of the 2D marker positions of the control column and pedals from the video sequences using low level image processing. Section 5 presents the elaborated methods to find the 3D positions of the control column and pedals which can be transformed to the positions of the control surfaces (actuator signals rudder, elevator and aileron) based on

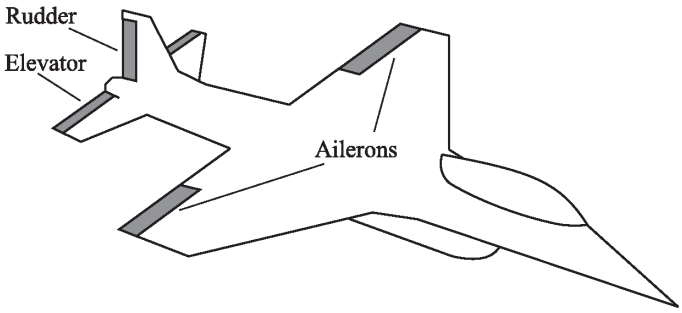

Fig. 3. Control surfaces of conventional airplane

their characteristics and a look-up table increasing the speed of computation. This section contains the camera calibration algorithm, the kinematic model of the control surfaces from robotics point of view and the look-up table construction. Section 6 deals with low level data conditioning including time scaling of the video sequences, resampling of magnetometer data and the computation of the aircraft velocity. The paper is ended with the conclusions and future research directions.

2 Control surface characteristics of the sailplane

By moving the control column forward and backward, the deflection of the elevator is changed according to a linear function, resulting in a change in pitch of the aircraft, that is a rotation around the Y_B axis, see Figure 4.

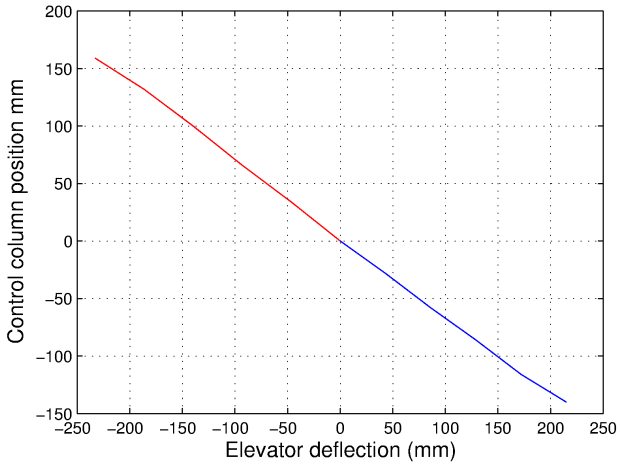

Fig. 4. Linear characteristic of the elevator - control column ensemble (forward-backward movement in mm)

By laterally moving the control column, the deflection of the ailerons is accomplished, resulting in a change in roll of the aircraft, or a rotation along the X_B axis with a certain degree of nonlinearity, see Figure 5.

The rudder is controlled using pedals and it is responsible for the change of yaw (heading) of the aircraft, that is the rotation along the Z_B axis with a linear characteristic (not drawn). The 2D marker positions of the pedals can immediately be converted to rudder positions based on the linear characteristic between them.

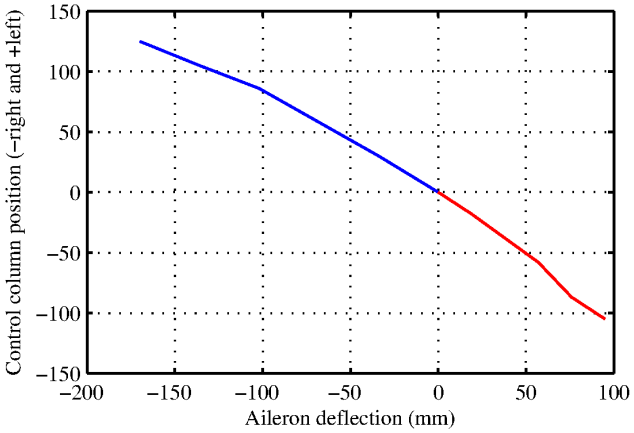

Fig. 5. Nonlinear characteristic of the aileron - control column ensemble (left-right movement in mm)

The above characteristics were identified in steady state situation before flight. The recorded flight was comprised of a winch launch, followed by four 90 degree left hand turns after which the glider landed parallel to its takeoff position with the use of its air-brakes. The pilot was the first author having pilot's licence for sailplanes.

3 Technical solutions for data gathering

Due to the fact that the secondary piloting post has flight controls (control column and pedals) identical to the first, by fixing visual markers on the flight controls and recording their movements during flight with a video camera, the positions of the control column and pedals can be determined using the recorded pixel values.

The camera was positioned on the cockpit's canopy facing down, allowing observation of the complete workspace of the control column and pedals. As from this position, the rudder control was obstructed from view; the visual marker had to be placed in the camera's field of view using a pushrod, see Figure 6.

Fig. 6. Inside of cockpit and visual markers as observed by the video camera

At the start of image recording and before takeoff, both the control column and the rudder controls were moved from endpoint to endpoint. This action coupled with the knowledge of

control surface characteristics results in the function relations between determined marker positions and control surface deflections.

4 Determining the 2D marker positions of control column and pedals using low level image processing

Differentiation between the flight controls was achieved using a white visual marker for the control column and a yellow one fixed to the rudder control's pushrod. At startup, the offline image processing algorithm firstly determines the correct sample rate (29.97 frames/sec), then it determines the marker positions frame by frame.

As aides, the use of workspaces was introduced, which are masks that allow only a certain portion of the frame to be analyzed. The control column's workspace is circular due to the fact that this control can be moved in any direction during flight and its center is determined by the previous marker position.

Because the rudder control's visual marker is only capable of translational movement, its workspace is a parallelogram and its position is also dependent on the marker's previous position, see Figure 7.

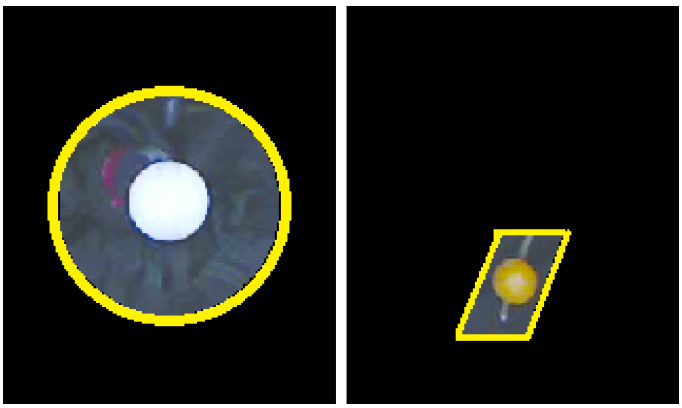

Fig. 7. Workspaces of the control column and rudder control

At startup, the positions of the two workspaces have to be determined manually after which the image processing algorithm determines the marker coordinates and workspace positions for the following frames. In exceptional instances, when the marker's positions cannot be determined, because of obstruction of one marker by the other, human intervention is necessary.

The use of two separate workspaces also helps determine local exposure metering which is exceptionally useful, due to the fact that during flight, the aircraft's orientation according to the Sun changes continuously. This constant change of lighting conditions results in the shading or full illumination of the visual markers thus changing their color and homogeneity, rendering successful image recognition set for a single color spectrum impossible.

The correlation of varying light intensity and unsuccessful image recognition can be observed in Figure 8 for column markers and in Figure 9 for rudder markers, respectively.

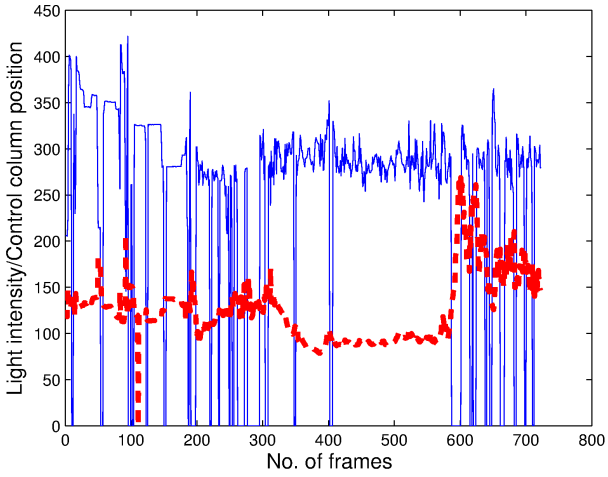

Fig. 8. Correlation between control column marker determination and varying lighting conditions (without corrections). Blue - marker position, red - light intensity

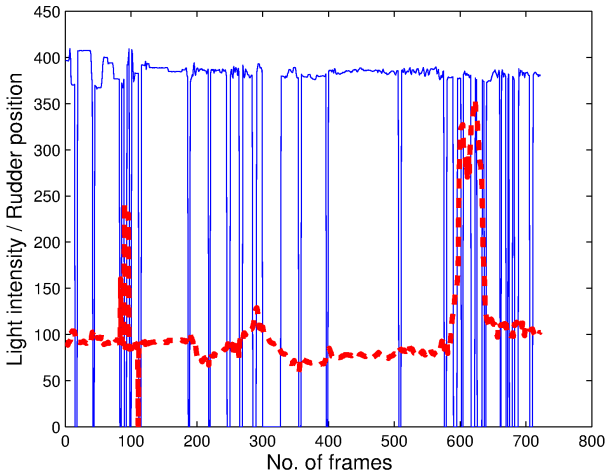

Fig. 9. Correlation between rudder control marker determination and varying lighting conditions (without corrections). Blue - marker position, red - light intensity

Exposure metering was accomplished by adding the pixel values of all three channels (Red + Green + Blue) in the current workspace, where the colors closer to white have a value closer to 1, and those closer to black having values closer to 0. In case of overexposed images, not only the markers were completely white, but also most parts of the background, resulting in the impossibility of marker recognition without corrective measures.

Following the determination of local exposure levels, the RGB format's 256 colors were simplified to only 6, improving marker separation from background whilst making the marker color appearing more homogeneous.

In case of underexposed workspaces, the white visual marker corresponding to the control column has white and gray colors. For successful marker recognition, of the six colors, both the whitest and second whitest colors have to be found (maximum red, green and blue). The merger of the background with the

marker is prevented by keeping the second whitest color in case it is only 51% darker than the first. Any darker, and only the whitest color is taken into account. In the case of normal- or overexposure only the whitest color is preserved.

In the following step, only the two selected colors are kept in a black and white image.

During the process, some artifacts remain, and for a complete marker separation, an erosion-dilation based routine was applied, the magnitude of which is determined dynamically, based on exposure metering.

After filtering, the algorithm searches for ellipse shaped objects with an eccentricity of less than 0.6 and an area close to that of the visual marker. If successfully found, the object's center is determined according to the ellipse's center of mass, otherwise manual correction is necessary.

The process is finished by drawing a crosshair on the marker's center of mass and plotting its circumference and saving the marker coordinates. The same procedure applies for determining the rudder control marker's positions, with slight differences. Three exposure levels are set in the current workspace. In case of a normally exposed workspace, the visual marker has an inhomogeneous yellow color. In this instance, the RGB color map is simplified to 5 colors of which the two colors closer to yellow are selected (maximal red, maximal green and minimal blue values).The second yellow color is taken into account only if it is more than 32% closer to yellow than the first one.

In the case of a slightly overexposed workspace, two colors prevail due to the marker's gleaming: white and yellow. Therefore the search is based on these two colors and only these two colors will be retained in the black and white rendition of the image. In case of a severely overexposed workspace, the yellow marker looks completely white and is very difficult to separate from the background, see Figure 10. In this case, the workspace is darkened and only the whitest color is taken into account for marker identification, see Figure 11.

Fig. 10. Severely overexposed image, with hardly recognizable visual markers

Before defining the marker position, the black and white image is enhanced by dynamically determined erosion-dilation filtering. Afterwards, the algorithm searches for elliptical objects

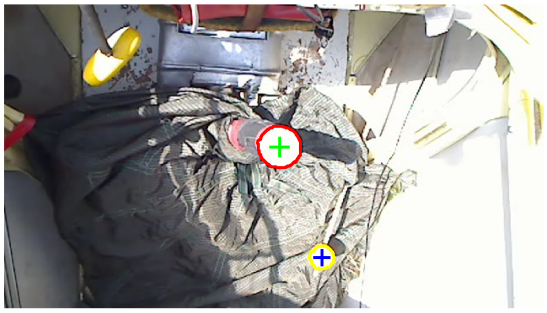

Fig. 11. Successfully determined marker positions in case of an overexposed image

with an eccentricity of less than 0.7 and an area close to that of the visual marker. The center of the visual marker is determined by finding the marker's center of mass.

The frame sequences are saved as video for a posteriori verification. The determined control column marker's positions can be seen in Figure 12 and Figure 13. The determined rudder pedal marker's positions are drawn in Figure 14.

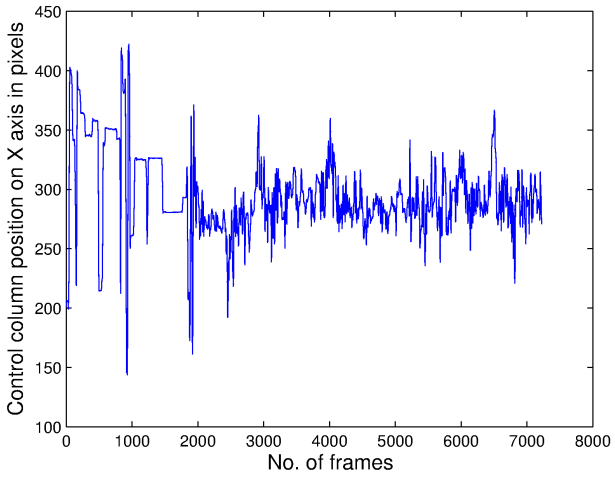

Fig. 12. Control column's positions along the X axis for the entire set of data

5 Determining the elevator and aileron positions using high level image processing

5.1 Camera calibration

The video camera's parameters are a priori determined with a chess-board like picture rendition therefore the camera's K calibration matrix is regarded as known. The problem lies in determining the homogeneous transformation between the video camera's K_C, and the aircraft's K_0 coordinate systems.

For this, a calibration object is needed that has various spatially placed visual markers, the origin of which coincides with one of the control column's known positions. This calibration object has 7 visual markers, of which 2 are not coplanar and 4 are in the same plane. The visual marker's reciprocal coordi-

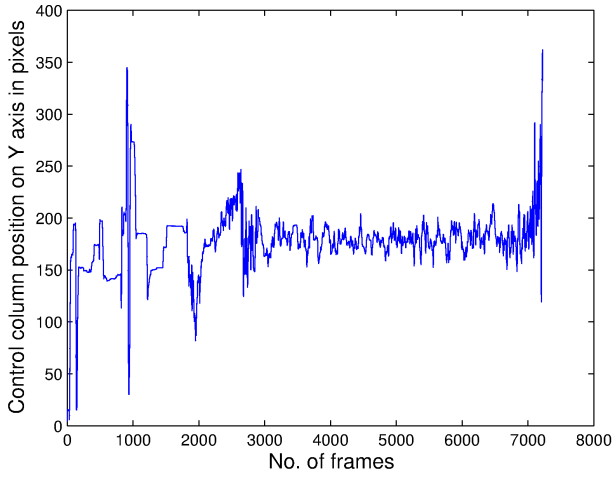

Fig. 13. Control column's positions along the Y axis for the entire set of data

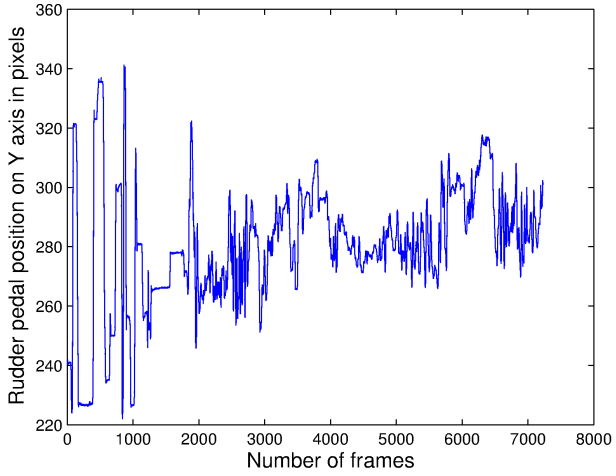

Fig. 14. The rudder control's positions for the entire set of data

nates are known, and the position and orientation of the video camera can be determined after the calibration process. During data collection, before takeoff the calibration object is temporarily placed in the cockpit and after the shots required for the offline calibration are completed, it is removed from the cockpit due to safety reasons.

Let's use r_i as the visual markers position in K_0; r_{ci} as the video camera's position in K_c, and $(u_i, v_i, w_i)^T$ as their coordinates in the camera sensor's plane. If the unknown homogeneous transformation between the camera and calibration object is defined by the orthonormal rotation matrix R and position t, then their relationship is:

$$\lambda_i K^{-1} \begin{pmatrix} u_i/w_i \\ v_i/w_i \\ 1 \end{pmatrix} = \lambda_i r_{ci} = R r_i + t \tag{1}$$

The appearance of the λ_i parameter is due to the fact that reprojecting the point from the sensor plane, there are infinite r_i points that form in the camera center. Otherwise, the relationship between the R and t parameters is linear. Thus considering for every r_{ci} its own perpendicular n_{i1} and n_{i2} vectors in the base of K_c, the relationship is substituted for the following linear homogeneous equation system for n_{ij}:

$$n_{ij}^T (R r_i + t) = 0, \quad j = 1,2 \;\; i = 1, \ldots N \tag{2}$$

Thus, if we have a number of $N \geq 6$ r_i points, then using the LS (Least Squares) method, an optimal R, t solution can be determined. Unfortunately it is not to be expected that the R matrix will be orthonormal; therefore the approximation of an orthonormal R of the optimal LS solution Q for R must be determined. This is an abstract optimization problem using a Frobenius norm and constraints:

$$\min_R \|R - Q\|_F \text{ such that } R^T R - I = 0 \tag{3}$$

The problem can be solved with the Lagrange multiplier method, where the Lagrange multiplier Λ is a symmetrical matrix. Transforming the problem to the form:

$$L = \text{trace}\left((R-Q)^T\right)(R-Q) + \left(R^T R - I\right)\Lambda) \tag{4}$$

and completing the derivations yields

$$R(I + \Lambda) = RS = Q \text{ and } (I + \Lambda) \text{ is symmetrical} \tag{5}$$

The solution can be determined with the use of singular value decomposition [7]:

$$Q^T Q := S^2 \rightarrow SVD \rightarrow S^2 = U_{S^2} \Sigma_{S^2} U_{S^2}{}^T \rightarrow S = U_{S^2} \Sigma_{S^2}^{1/2} U_{S^2}{}^T$$

$$R_{opt} = Q S^{-1} \tag{6}$$

Knowing the resulting R_{opt}, the previous linear equation can be considered when the R_{opt} has a fixed value, which can be solved again for t_{opt} using the LS method.

The results for R_{opt} and t_{opt} can be further refined using constrained nonlinear numerical optimization techniques.

Determining the control column's 3D marker positions from 2D pixel values requires the knowledge of the video camera's calibration matrix - previously determined by identification - and the control column's physical characteristics.

5.2 The control column's kinematic model

As a consequence of the kinematic model of the control column - control surface structure, the visual marker fixed to the control column does not determine a regular spherical surface. The kinematic model of the 2 Degree-Of-Freedom (DOF) structure is shown in robotic view in Figure 15 where $l_2 = 420mm$, $l_1 = 80mm$ and $d = 100mm$ are the distances in the joint model and α, β are the joint variables.

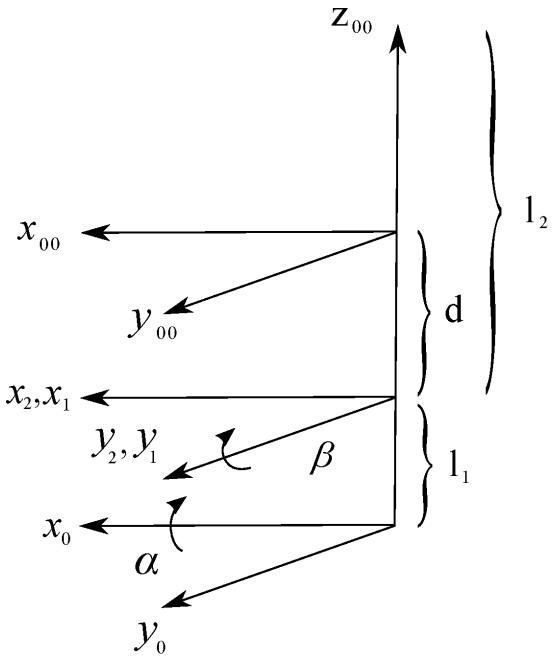

Fig. 15. Kinematic model of the control column

According to the control column's kinematic model following relations can be derived:

$$T_{01} = \begin{bmatrix} 1 & 0 & 0 & 0 \\ 0 & C_\alpha & -S_\alpha & -S_\alpha l_1 \\ 0 & S_\alpha & C_\alpha & C_\alpha l_1 \\ 0 & 0 & 0 & 1 \end{bmatrix} \tag{7}$$

$$T_{12} = \begin{bmatrix} C_\beta & 0 & S_\beta & 0 \\ 0 & C_\alpha & 0 & 0 \\ -S_\beta & S_\alpha & C_\beta & 0 \\ 0 & 0 & 0 & 1 \end{bmatrix} \tag{8}$$

where S_α,C_α etc. stand for $sin(\alpha)$, $cos(\alpha)$.

By knowing the l_1, l_2 and d distances and α and β joint angles, the T_{02} homogeneous transformation and the dependence of visual marker's 3D position on α and β can be determined:

$$T_{02} = T_{01} \cdot T_{02} = \begin{bmatrix} C_\beta & 0 & S_\beta & 0 \\ S_\alpha S_\beta & C_\alpha & -S_\alpha C_\beta & -S_\alpha l_1 \\ -C_\alpha S_\beta & S_\alpha & C_\alpha C_\beta & C_\alpha l_1 \\ -0 & 0 & 0 & 1 \end{bmatrix} \tag{9}$$

$$T_{02} \begin{pmatrix} 0 \\ 0 \\ l_2 \\ 1 \end{pmatrix} = \begin{pmatrix} S_\beta l_2 \\ -S_\alpha C_\beta l_2 - S_\alpha l_1 \\ C_\alpha C_\beta l_2 + C_\alpha l_1 \\ 1 \end{pmatrix} = \begin{pmatrix} x_0 \\ y_0 \\ z_0 \\ 1 \end{pmatrix} \tag{10}$$

$$\begin{pmatrix} x_{00} \\ y_{00} \\ z_{00} \end{pmatrix} = \begin{pmatrix} x_0 \\ y_0 \\ z_0 - (l_1 + d) \end{pmatrix} \tag{11}$$

Notice that K_0 with axes x_0, y_0, z_0 is an inertial frame while K_{00} with axes x_{00}, y_{00}, z_{00} is its shifted version considered as the aircraft's reference coordinate system for our purposes. For simplicity, the 3D coordinates of the control column marker according to equation (11) are also denoted by x_{00},y_{00} and z_{00}, respectively.

5.3 Look-up table construction for inverted control position determination

Since the control column's α and β range spans to ±30° and ±20°, respectively, the workspace of the control column is determined by the $x_{00}(\alpha,\beta)$, $y_{00}(\alpha,\beta)$, $z_{00}(\alpha,\beta)$ surfaces, respectively, shown in Figures 16, 17, and 18 (vertical axes in mm). They illustrate the relation between joint variables α, β and the three coordinates of the 3D position of the control column. They follow from the control column's kinematic model, see equations (9)-(11). The characteristics $x_{00}(\alpha,\beta)$, $y_{00}(\alpha,\beta)$ and $z_{00}(\alpha,\beta)$ are valid in every situations. For the parameters of the kinematic model the first two surfaces are almost linear while the third one is nonlinear. Unfortunately, α, β cannot be measured, they should be determined by using image processing.

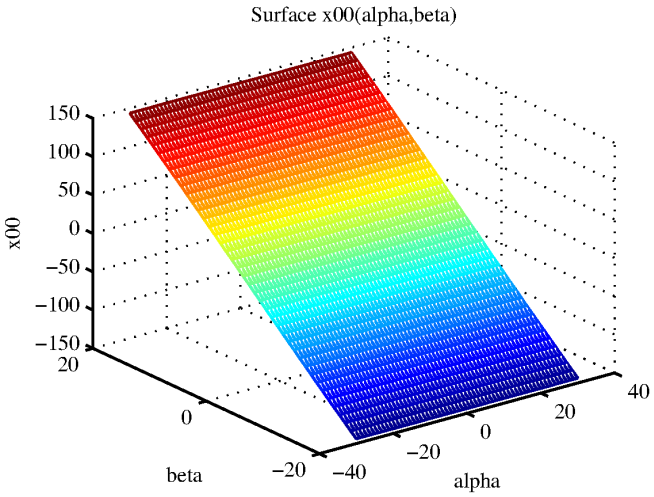

Fig. 16. The $x_{00}(\alpha,\beta)$ surface determined by control column

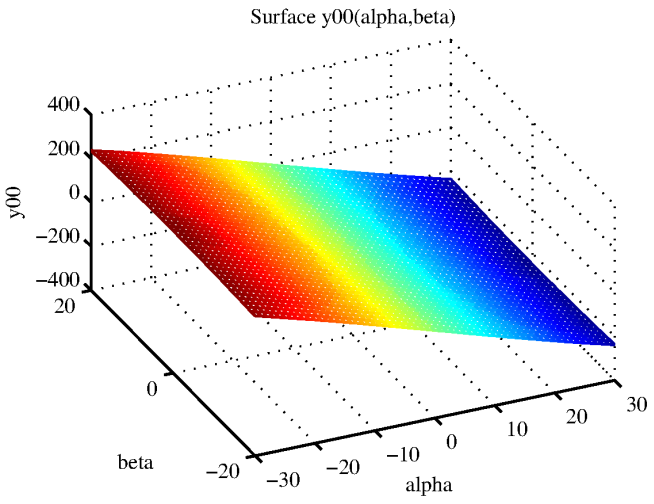

Fig. 17. The $y_{00}(\alpha,\beta)$ surface determined by control column

As a result of the control column's kinematics, according to several α and β angles, the control column's visual marker position $r = (x_{00}, y_{00}, z_{00})^T$ can be determined based on the coordinate systems, matrices and vectors drawn in Figure 19.

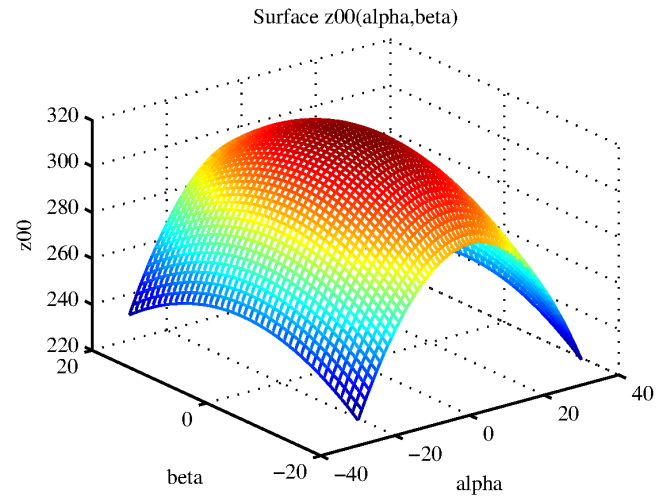

Fig. 18. The $z_{00}(\alpha,\beta)$ surface determined by control column

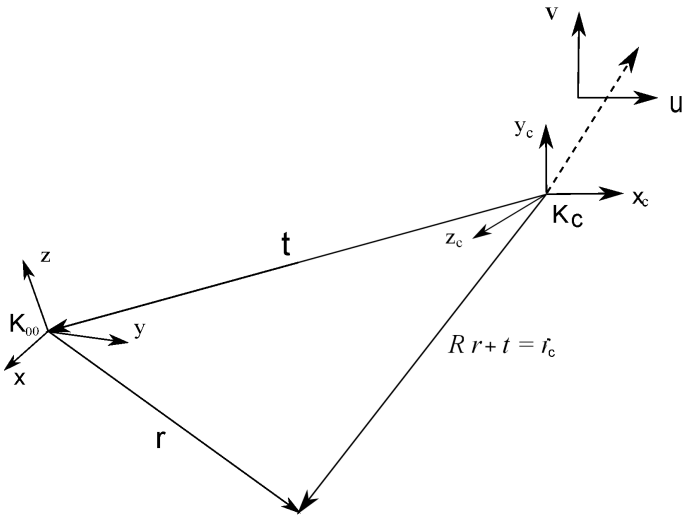

Fig. 19. Relations between the camera's coordinate system and the aircraft's coordinate system

K_c - the camera's coordinate system

K_{00} - the aircraft's coordinate system

R_{opt} - optimal orientation matrix of the video camera

r - vector pointing from the origin K_{00} to the marker position, expressed in the base of K_{00}

t_{opt} - vector pointing form the K_c origin to the K_{00} origin, expressed in the base of K_c

r_c - vector pointing form the control column's marker position to the K_c origin, expressed in the base of K_c

From here, the following expressions can be determined, expressed in the base of K_c:

$$r_c = R_{opt} r + t_{opt} \tag{12}$$

To be able to determine the u,v, w values formed in the camera plane expressed in the base of K_c, for any given angle, we apply the K calibration matrix:

$$(u,v,w)^T = K(R_{opt} r + t_{opt}) \tag{13}$$

The u, v and w values of $(u,v,w)^T$ are divided by w, and by applying the inverse of the K camera matrix, we can determine the vector pointing from the video camera's center point to the control column's visual marker in the base of K_c which is normalized for later steps:

$$r_{cb} = K^{-1} \begin{pmatrix} u/w \\ v/w \\ 1 \end{pmatrix} \tag{14}$$

$$r_{cb} := r_{cb} / \|r_{cb}\| \tag{15}$$

As an example, for the numerical values of $\alpha = -20°$ and $\beta = 25°$, the r_{cb} direction unit vector's coordinates for the look-up table are:

$$r_{cb} = \begin{pmatrix} 0.2058 \\ -0.1949 \\ 0.9590 \end{pmatrix} \tag{16}$$

For the fine resolution of (α,β) pairs we can compute a look-up table as follows:

$$(\alpha,\beta) \xrightarrow[\text{kinematics}]{\text{2DOF}} (x_{00}, y_{00}, z_{00}) \xrightarrow{R_{opt}, t_{opt}, K} (u,v) \xrightarrow{K^{-1}} r_{cb} \tag{17}$$

The r_{cb} unit vector has the direction of the straight line starting in the point $(u,v,1)^T$ and going through the camera center and ended on the $r(\alpha,\beta)$ surface. For this computation a single camera is satisfactory.

Hence, having constructed the look-up table (LUT), we can compute from the 2D pixel positions (u,v) the unit vector r_{cb}, then (α,β) belonging to r_{cb} according to the look-up table, then the 3D position (x_{00}, y_{00}, z_{00}) of the control column identifying its forward/backward and left/right movement and from it the position of the control surfaces by using the control surface characteristics:

$$(u,v,1) \xrightarrow{K^{-1}} r_{cb} \xrightarrow{\text{LUT}} (\alpha,\beta) \xrightarrow[\text{kinematics}]{\text{2DOF}} (x_{00}, y_{00})$$
$$(x_{00}, y_{00}) \xrightarrow{\text{control characteristics}} (\text{elevator, aileron}) \tag{18}$$

The rudder positions can immediately be determined from the 2D pixel values of the pedal's marker.

5.4 Experimental results of the computation of elevator and aileron positions

Based on the elaborated method and the look-up table, the elevator and aileron positions of the actuators have been determined. Figures 20 and 21 illustrate the relation between the 2D marker positions of the control column and the elevator and aileron positions, respectively.

Similarly, Figures 22 and 23 illustrate the same relations from another view point, namely, the relation between the x_{00}, y_{00} components of the 3D positions of the control column and the elevator and aileron positions, respectively.

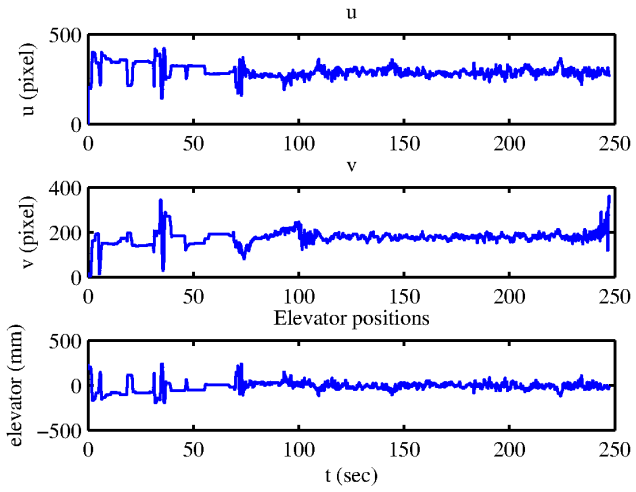

Fig. 20. Relation between the control column's pixel coordinates and the elevator positions

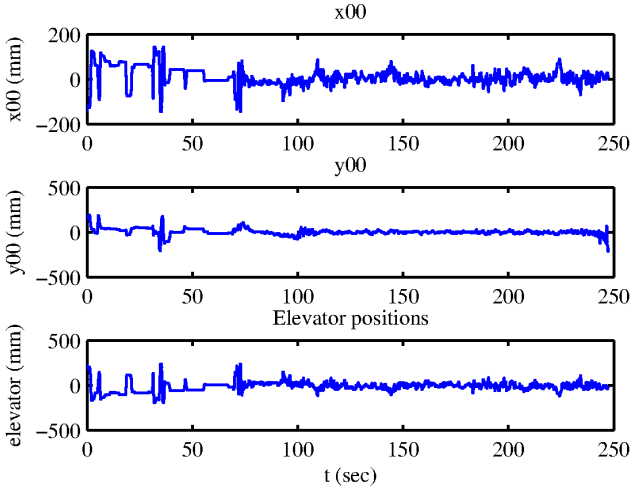

Fig. 22. Relation between the control column's 3D coordinates and the elevator positions

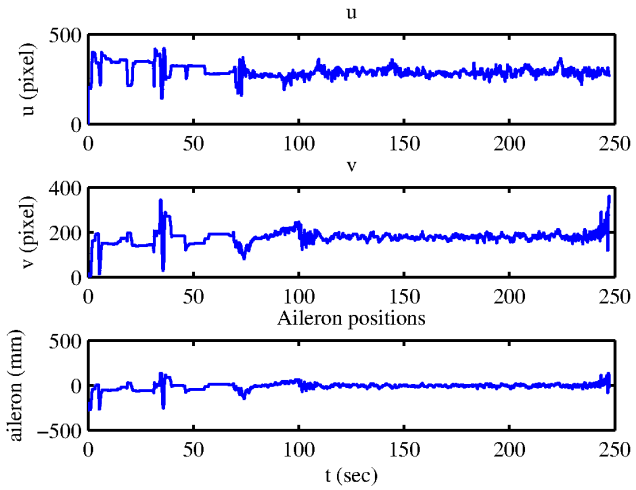

Fig. 21. Relation between the control column's pixel coordinates and the aileron positions

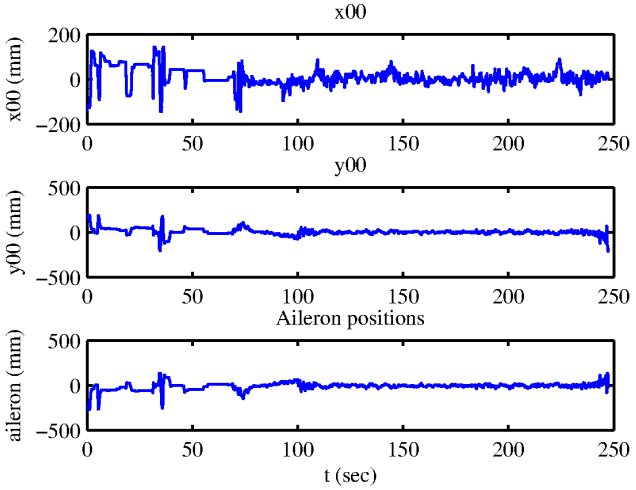

Fig. 23. Relation between the control column's 3D coordinates and the aileron positions

Figures 24 and 25 show the computed actuator positions as input records for identification purposes. Time conditioning of video sequences (see later on) was also taken into consideration. Free flight for identification is between 101s (release) and 246s (landing).

6 Primary data conditioning

The data acquisition was performed using two HW/SW systems deployed to the sailplane before flight. Data logging of GPS, IMU and magnetometer sensors was performed on a system containing the sensors and running under Linux allowing time resolution of 100 microseconds under control [3], [8]. Sensor measurement contained high precision time stamps. Video sequences of control column and pedal markers were collected on a separate system running under Windows XP allowing slower time resolution which was slowly drifting.

6.1 Time conditioning of video sequences

The start time of video sequences was exactly defined for the Linux system in a manually controlled way and from this time instant the video sequence was recorded with a fixed frequency of 29.97 frames/sec defined by the video camera and Windows XP. To the video sequences marker-labels were added defining the start of image recording, the start of towing of the sailplane, the beginning of release and free flight, the beginning of deploying the air-brakes, the landing and the stopping. These markers were added in a manually controlled process.

Because the two operating systems could not be synchronized and precise time measurement under Windows XP was not possible, the slowly varying video frequency was compensated in such a way that a scaling factor was defined based on the IMU's 3D accelerometer record. This technique uses the possibility that the time of release and landing can be determined with high precision from the 3D acceleration record and the time stamps.

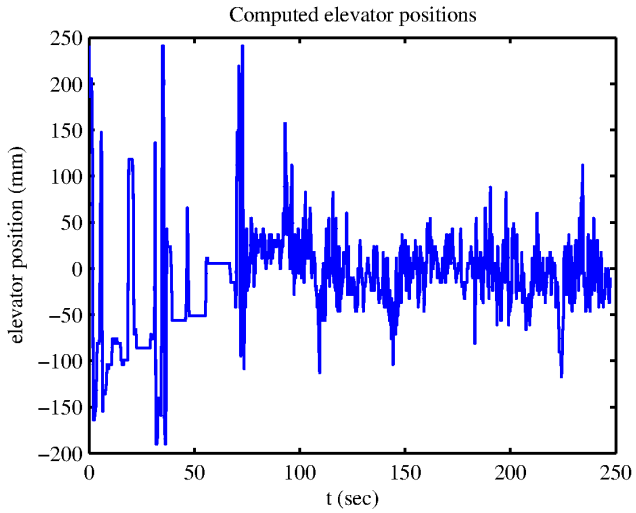

Fig. 24. The record of computed elevator signals

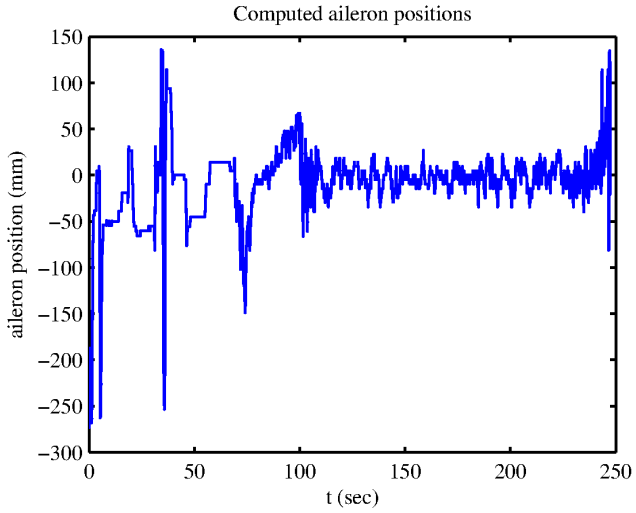

Fig. 25. The record of computed aileron signals

Hence, by using the scaling factor, the time interval between release and landing can be defined with high precision. On the other hand, this is the competent interval for latter dynamic model identification. The corrected records are drawn in Figure 26.

6.2 Low level signal processing of GPS, IMU and magnetometer data

The nominal sampling times of sensors were 20ms for IMU's 3D acceleration and 3D angular velocity, 50ms for 3D magnetometer and 1s for GPS position. The first task of low level signal processing was to compensate the slow fluctuation of the measurement times which was solved by giving preference of the sensor frequencies against the time stamps.

The magnetometer measurements were obtained in Gauss, but for future applications they were converted to micro Tesla. Another problem was the different frequencies of IMU and magnetometer sensors while for state estimation equal frequencies are preferable. Therefore the 3D magnetometer data were interpo-

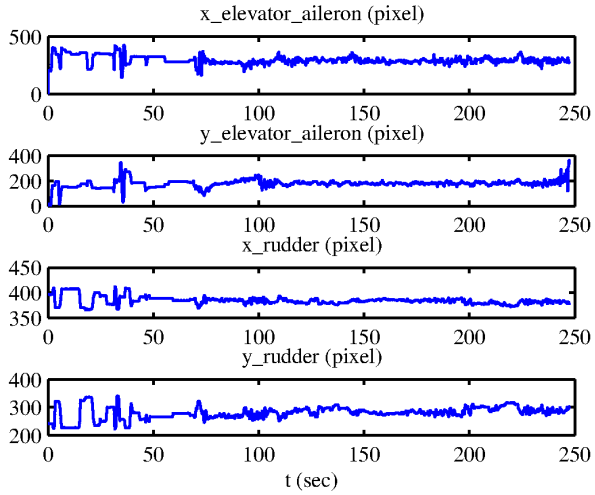

Fig. 26. Time scaled records of control column and rudder markers

lated and resampled using MATLAB's function *interp* assuring 20ms sampling time, see Figure 27. As can be seen, the original and resampled data are well covered.

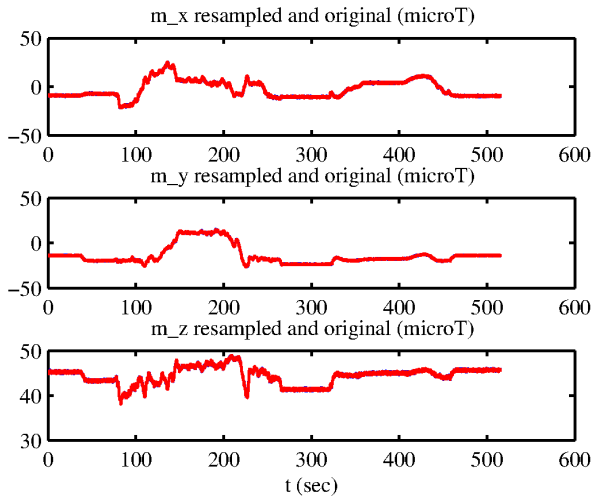

Fig. 27. Interpolated and resampled magnetometer data

The GPS position $r = (x, y, z)^T$ of the sailplane has large magnitude ($6.37 \cdot 10^6$ m) in the ECEF frame hence the usual way is to introduce the nearest point Q on the rotational ellipsoid to the body frame ACB, see Figure 1, and characterize the position of the NED frame as $p = (\varphi, \lambda, h)^T$ where φ, λ and h are the geodetic latitude, longitude and hight, respectively. This conversion can be performed by using the following algorithm, see [4]:

$$(x, y, z)^T \rightarrow (\varphi, \lambda, h)^T \tag{19}$$

Initialization:

$$h := 0,\ N := a,\ p := \sqrt{x^2 + y^2},\ T_\lambda = y/x \xrightarrow{\text{atan}} \lambda$$

Cycle:

$$S_\varphi := \frac{z}{N(1-e^2)+h}, \quad T_\varphi := \frac{z+e^2 N S_\lambda}{p} \xrightarrow{\text{atan}} \varphi$$
$$N := \frac{a}{\sqrt{1-e^2 S_\varphi^2}}, \quad h := \frac{p}{C_\varphi} - N$$

where $a = 6378137.0$m is the main axis and $e = 0.0818$ is the eccentricity of the rotational ellipsoid of the Earth. By experiences, the convergence is quicker if φ is computed by atan instead of asin, convergence to cm precision requires 25 iterations.

State estimation needs also the information of the aircraft's velocity derived from GPS position. Typical state estimation methods use the velocity $v_b^n = (v_N, v_E, v_D)^T$ expressed in the NED frame. For this purpose $r_b^e = (x, y, z)^T$ has to be differentiated in the ECEF frame and transformed to the NED frame.

The numerical differentiation was based on the MATLAB's function *sgolay* which is a Savitzky-Golay (polynomial) FIR smoothing filter returning also the matrix of differentiation filters. Some modifications were implemented in our *diffsgolay* extension handling correctly the initial and ending part of the records.

First the velocity of ACF was determined using numerical differentiation in the ECEF frame in the form of $v_b^e = (\dot{x}, \dot{y}, \dot{z})^T$, then it was transformed into the NED frame using the rotation matrix $R_e^n(\varphi, \lambda)$ resulting in the velocity of the body frame expressed in the NED frame [4]:

$$v_b^n = R_e^n(\varphi, \lambda) v_b^e$$
$$\begin{pmatrix} v_N \\ v_E \\ v_D \end{pmatrix} = \begin{bmatrix} -C_\lambda S_\varphi & -S_\lambda S_\varphi & C_\varphi \\ -S_\lambda & C_\lambda & 0 \\ -C_\lambda C_\varphi & -S_\lambda C_\varphi & -S_\varphi \end{bmatrix} \begin{pmatrix} \dot{x} \\ \dot{y} \\ \dot{z} \end{pmatrix} \qquad (20)$$

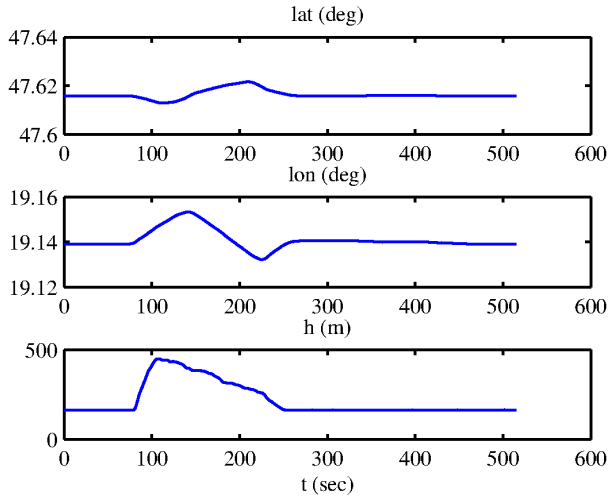

Fig. 28. Sailplane position expressed in NED frame

From DGPS reasons two GPS receivers were applied. The second GPS antenna was in the tight neighborhood of the IMU sensor hence its measurement was considered as the airplane position. The deployed GPS system used also carrier phase measurements in order to increase the precision [8]. The airplane's

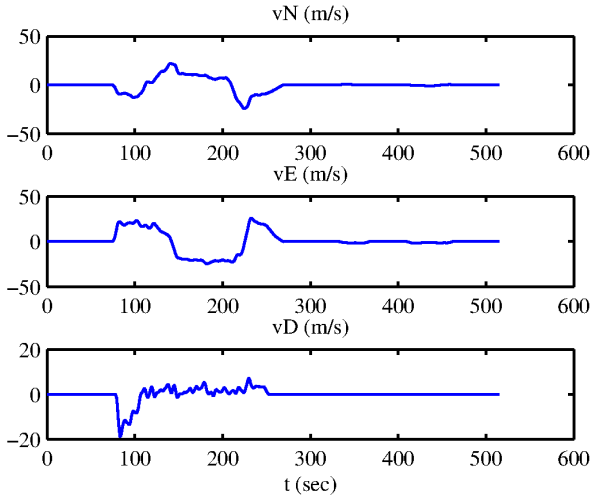

Fig. 29. Sailplane velocity expressed in NED frame

position and velocity records expressed in NED frame are shown in Figure 28 and Figure 29.

State estimation methods should take into consideration that ECEF is not an inertial frame since it rotates around the z-axis of the quasi-inertial frame ECI with angular velocity $\omega_E = 7.2921151467 \times 10^{-5}$rad/s, while the IMU measurements are relative to the inertial frame. Especially, if the aircraft is standing (steady state) then the IMU measures the negative gravity acceleration pointing upwards. The differences between ECEF and ECI are important for high speed maneuvering. It can be remarked here that applying 3 GPS receivers and appropriate signal processing the angle of attack and sideslip angle could be estimated too.

7 Conclusions

The paper presented a system engineering method used for data acquisition of GPS, IMU and pilot control signals.

The flight of the airplane was influenced by the control column and pedal manipulated by the pilot whose positions can only visually be observed. For the time of data logging, an external sensory system (GPS, IMU, magnetometer) and a camera system were deployed on the airplane supporting the collection of flight data for state estimation and model identification. For determination of the control surface positions from video sequences of the control column and pedal markers an algorithm was developed and discussed in detail. The 3D positions of the pilot's control column are determined from 2D pixel values based on a look-up table derived from the 2 DOF kinematic model of the mechanism and the calibrated camera model. Low level signal processing of GPS, IMU and magnetometer data conditioning was presented.

The approach can be applied for any aircraft in the initial phase of control system design when no onboard navigation and actuator sensors are available.

The steps for further developments lie in the elaboration of high precision state estimation methods in the presence of noises

and identification algorithms to find the aircraft's nonlinear dynamic model, its unknown functional relations and their parameters. Their research is in progress and the results will be published in next papers.

References

1 **Klein V, Morelli EA**, *Aircraft System Identification, Theory and Practice*, Virginia, American Institute of Aeronautic and Astronautics, 2006.

2 **Farrell J**, *Aided Navigation. GPS with High Rate Sensors*, New York, McGraw-Hill Companies, 2008.

3 **Kis L, Lantos B**, *Sensor Fusion and Actuator System of a Quadrotor Helicopter*, Periodica Polytechnica Electrical Engineering, **53**(3-4), (2009), 139-150, DOI 10.3331/pp.ee.2009-3-4.06.

4 **Lantos B, Márton L**, *Nonlinear Control of Vehicles and Robots*, London, Springer-Verlag, 2011, DOI 10.1007/978-1-84996-122-6.

5 **Bonnabel S, Martin P, Rouchon P**, *Symmetry-Preserving Observers*, IEEE Transaction on Automatic Control, **53**(11), (2008), 2514-2526, DOI 10.1109/TAC.2008.2006929.

6 **Hartley R, Zisserman A**, *Multiple View Geometry in Computer Vision*, Cambridge, Cambridge University Press, 2003.

7 **Tél F**, *Stereo Image Processing System for Robotic Applications*, PhD Thesis. Budapest University of Technology and Economics, Department of Control Engineering and Information Technology, Budapest, 2009.

8 **Kis L, Lantos B**, *Aided Carrier Phase Differential GPS for Attitude Determination*, In: Proceedings of IEEE/ASME International Conference on Advanced Mechatronics AIM2011, Budapest, 2011, pp. 778-783, DOI 10.1109/AIM.2011.6027009.